LETTERS
DOI: 10.1038/s41550-017-0217-y

nature astronomy

The nature of solar brightness variations

A. I. Shapiro[1*], S. K. Solanki[1,2], N. A. Krivova[1], R. H. Cameron[1], K. L. Yeo[1] and W. K. Schmutz[3]

Determining the sources of solar brightness variations[1,2], often referred to as solar noise[3], is important because solar noise limits the detection of solar oscillations[3], is one of the drivers of the Earth's climate system[4,5] and is a prototype of stellar variability[6,7]—an important limiting factor for the detection of extrasolar planets. Here, we model the magnetic contribution to solar brightness variability using high-cadence[8,9] observations from the Solar Dynamics Observatory (SDO) and the Spectral And Total Irradiance REconstruction (SATIRE)[10,11] model. The brightness variations caused by the constantly evolving cellular granulation pattern on the solar surface were computed with the Max Planck Institute for Solar System Research (MPS)/University of Chicago Radiative Magnetohydrodynamics (MURaM)[12] code. We found that the surface magnetic field and granulation can together precisely explain solar noise (that is, solar variability excluding oscillations) on timescales from minutes to decades, accounting for all timescales that have so far been resolved or covered by irradiance measurements. We demonstrate that no other sources of variability are required to explain the data. Recent measurements of Sun-like stars by the COnvection ROtation and planetary Transits (CoRoT)[13] and Kepler[14] missions uncovered brightness variations similar to that of the Sun, but with a much wider variety of patterns[15]. Our finding that solar brightness variations can be replicated in detail with just two well-known sources will greatly simplify future modelling of existing CoRoT and Kepler as well as anticipated Transiting Exoplanet Survey Satellite[16] and PLAnetary Transits and Oscillations of stars (PLATO)[17] data.

In this study, we employed and combined the newest observations and modelling techniques to reproduce total solar irradiance (TSI) variability with high precision at all timescales from minutes to decades. We computed the magnetic component of the TSI variability with the Spectral And Total Irradiance REconstruction for the satellite era (SATIRE-S) model[10], which is one of the most successful and refined models of magnetically driven solar irradiance variability[4,9]. The high-cadence solar magnetograms and continuum images recorded by the Helioseismic and Magnetic Imager onboard the Solar Dynamics Observatory (SDO/HMI)[18] allowed us to expand SATIRE-S calculations of magnetically driven TSI variability to timescales of as little as 12 min (see Methods). Our calculations of the granulation-driven TSI variability were based on recent three-dimensional simulations[19] of convective gas currents both above and below the solar surface with the MPS/University of Chicago Radiative MHD (MURaM)[12] code (see Methods). Therewith we are able to cover timescales of hours, critical for exoplanet detection studies but less understood until now[20], with much better accuracy than was possible before[21] (see Methods). We also stress that, unlike empirical approaches[20,21], our calculations of the granulation were purely physics based, leaving us little freedom to change the properties of the granulation to match the observations.

Some statistical models[20] of TSI variability account for larger convective structures, such as supergranules and mesogranules. However, there is currently no evidence that these structures have an intrinsic brightness contrast of non-magnetic origin[22] so we did not include them in our modelling. We also refrained from including oscillations (which dominate TSI variability for periods of about 5 min and have been extensively used for helioseismology) in our modelling and focused on the TSI variations considered in helioseismology as noise.

While the amplitude of the granulation component of the TSI variability does not depend on time, the magnetic component is linked to the specific configuration of faculae (that is, bright concentrations of magnetic field[23]) and spots on the visible solar disk, and thus depends on solar magnetic activity. Therefore, we considered four intervals of the TSI record representing different levels of activity (Table 1). The three 1 month intervals at 2-min cadence allowed the study of the high-frequency component of the variability (Fig. 1), whereas the 19 year interval with a daily cadence was used to assess long-term changes.

Our calculations show that the TSI variability on timescales of 5 h (dashed lines in Fig. 1b,e,h) or less was entirely due to the granulation. The power spectrum was almost flat at periods of between 1 and 5 h (except for statistical noise). For periods of less than 1 h, the power decreased with frequency due to the increasing coherence between the granulation patterns. Since the period corresponding to the transition between the flat and decreasing parts of the power spectrum depends on the mean granule lifetime and size[21], the power spectra of stellar variations, observed by the Kepler and CoRoT (and in the future, the TESS and PLATO) missions, could provide a sensitive tool for determining the properties of stellar granules.

Both the granulation and the magnetic components of the TSI variability are important on timescales of 5–24 h, while at longer periods the TSI variability is dominated by the magnetic field. To better illustrate the role of faculae and spots, we separately plotted the magnetically driven variability due to spots and faculae.

Interestingly, while the TSI varied at a level of 200 ppm on timescales of minutes and exhibited significantly larger variations on timescales of days, transits of inner planets across the solar disk (in particular, Venus) could clearly be distinguished from solar noise in the TSI data[2] (and, independently, the Kepler mission has discovered Earth-sized planets). Our modelling explains this curious fact: magnetically driven TSI variations on timescales of planetary transits are small, whereas granulation-driven variations can be averaged out by smoothing the TSI over time. For late-type stars, the threshold timescale between granulation- and magnetically driven brightness variations is expected to be a function of the magnetic activity and, consequently, the rotational period (compare the

[1]Max-Planck-Institut für Sonnensystemforschung, Justus-von-Liebig-Weg 3, 37077 Göttingen, Germany. [2]School of Space Research, Kyung Hee University, Yongin, Gyeonggi 446-701, Korea. [3]Physikalisch-Meteorologishes Observatorium Davos, World Radiation Centre, 7260 Davos Dorf, Switzerland.
*e-mail: shapiroa@mps.mpg.de

Table 1 | Intervals of the TSI evolution considered in this study

Interval	Period	Cadence	Solar activity
October 2010	4 October 2010 to 31 October 2010	2 min	Low
August 2011	23 July 2011 to 16 August 2011	2 min	Transit of a large sunspot group
August 2012	10 August 2012 to 1 September 2012	2 min	High facular; low spot coverage
Long	1 January 1996 to 6 April 2015	1 day	Most of solar cycles 23 and 24

crossings between the green and black lines in Fig. 1b,e,h), surface gravity[24] and spectral class.

To test our calculations against observations, we utilized TSI time series obtained by the PREMOS instrument[25] onboard the PICARD mission and the VIRGO instrument[26] onboard the Solar and Heliospheric Observatory (SOHO). The PREMOS and VIRGO data are complementary in the sense that they allow reliable calculation of the TSI power spectra on timescales longer and shorter than 3.5 h, respectively (see Methods). Consequently, we created PREMOS/VIRGO composite TSI power spectra (see Methods and Supplementary Fig. 1) for the three 1 month intervals considered in this study.

The model reproduced the power spectra of the TSI in August 2011 and August 2012 remarkably well (Fig. 1f,i). The deviation at timescales of about 5 min was due to p-mode oscillations, which were not included in our model. For the October 2010 interval, the agreement worsened somewhat at timescales of about 10–20 h, which might be a signature of overcorrection of the SDO/HMI data for the orbital velocity (see Methods and Supplementary Fig. 2).

We merged (Fig. 2) the power spectra calculated for the August 2011 interval (keeping its 4 min to 7 days part) and the 'long' interval (the 7 days to 19 years part). On the observational side, we merged corresponding parts of the PREMOS/VIRGO composite power spectrum for August 2011 and the power spectrum calculated employing TSI values from the Physikalisch-Meteorologisches Observatorium Davos (PMOD) composite[27], which is a de facto standard observational dataset of daily TSI time series.

Our calculations accurately reproduced observed TSI variability on timescales covering more than six orders of magnitude (4 min to 19 years), over which the power spectral density changed by eight orders of magnitude (Fig. 2). Thus, the joint action of granulation and the magnetic field fully explained the TSI variability (excluding the 5-min oscillation component). The remarkable agreement between the model and the measurements (see Methods and

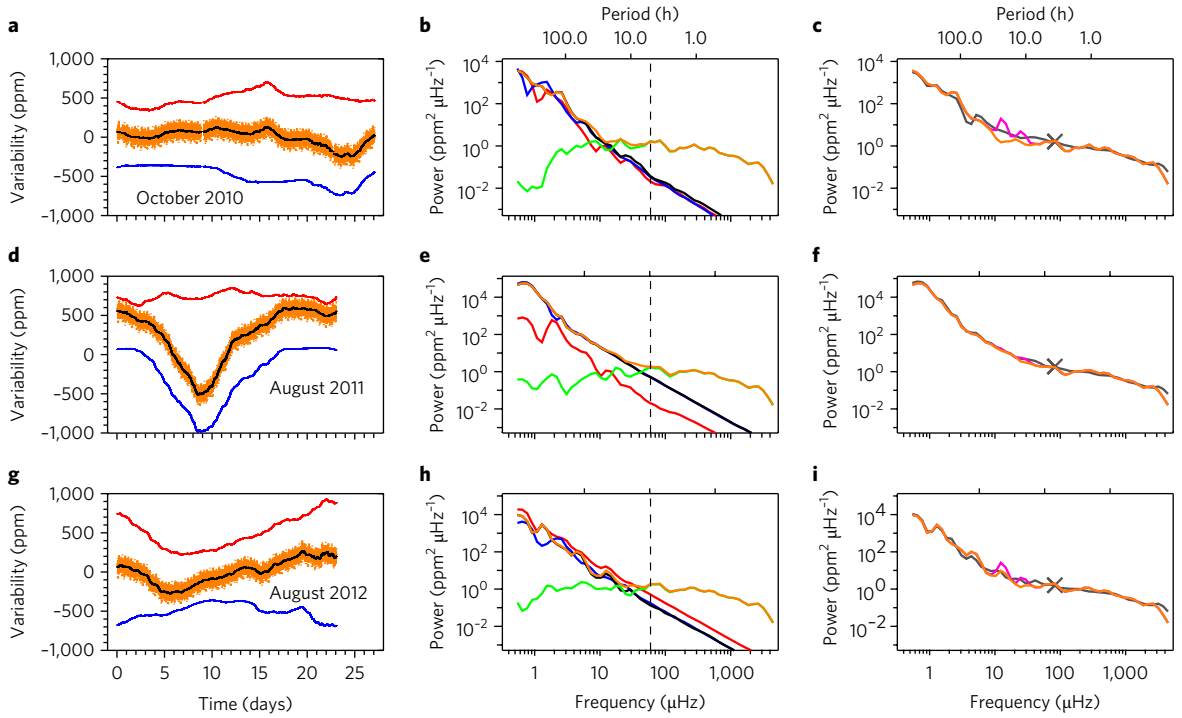

Fig. 1 | Short-term TSI variability at three intervals of very different activity level and variability of the Sun. a,**d**,**g**, Calculated TSI variations (orange), as well as calculated total magnetic (black), facular (red) and spot (blue) contributions to the TSI variation for the three 1-month intervals listed in Table 1. The plotted curves have been offset around zero for clarity. **b**,**e**,**h**, Global wavelet power spectra of the calculated TSI variations. In addition to the variability components shown in **a**,**d**,**g**, the granulation components (green) are plotted. Note that the green lines are not visible below 5 h (indicated by the vertical dashed lines) since they are covered by the orange lines. **c**,**f**,**i**, Global wavelet power spectra of the observed (grey) and modelled (orange and magenta) TSI variations. Plotted are the TSI variations calculated with and without correcting HMI data for the orbital velocity (orange and magenta curves, respectively). The difference between the orange and magenta curves indicates the uncertainty of the modelled power spectra due to the Doppler shift caused by the SDO orbital velocity (see Methods). The cross indicates the threshold between the PREcision MOnitoring Sensor (PREMOS) and Variability of solar IRradiance and Gravity Oscillations (VIRGO) segments of the observed wavelet power spectra. See Methods for a full description of the observed and modelled datasets, together with their uncertainties.

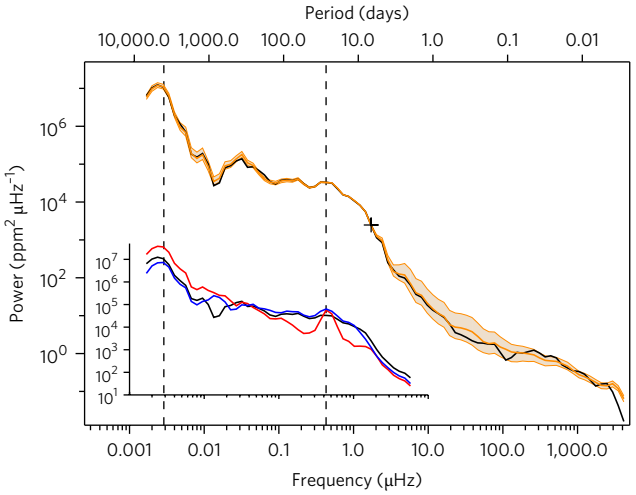

Fig. 2 | TSI variability on timescales from 4 min to 19 years. Main panel, power spectra of modelled (black) and measured (orange) TSI variations. The plus sign indicates the threshold between power spectra for the 1996–2015 and August 2011 time intervals (see Methods for details). The shaded areas, constrained by thin orange lines, indicate the estimated 1σ error intervals plotted around the measured power spectrum. Between 8 h and 2 days, the error intervals are interpolated, as a direct calculation of the error was not possible (see Methods). Inset: magnetically driven TSI variations calculated with daily cadence (black) and their facular (red) and spot (blue) components. The vertical dashed lines indicate the 11 year and 27 day periods.

Supplementary Fig. 3) cogently demonstrates that our understanding of these mechanisms—and the TSI variability in general—is fundamentally correct.

Our model allows us to separately look at the magnetically driven variability associated with spots and faculae. The transition between faculae- and spot-dominated regimes of the TSI variability occurred at a timescale of about one year (Fig. 2). Although magnetic TSI variations at timescales of less than one year were primarily due to spots, the contribution of faculae to the TSI variability was still rather significant and comparable to that of spots at timescales of 2–7 days, as well as at the solar rotational period, 27 days. The amplification of the facular signal at timescales of 2–7 days was associated with the strong dependence of the contrast of faculae on their position on the visible solar disk[28], while the peak at 27 days was attributed to long-lived large concentrations of faculae (whose lifetime can be up to several solar rotation periods).

Interestingly, the pronounced 27-day peaks in spot and facular components of TSI variability essentially cancelled each other out so that the total power spectrum was almost flat around the 27-day period. This implies that white light observations are not well suited for determining periods of stars similar to the Sun, and explains the poor performance of standard methods of period determination for stars older than the Sun[29].

The success of our model in replicating observed TSI variations using two well-understood components might be considered as a proof of concept for developing a similar model for Sun-like stars (which we define here as main sequence stars of spectral classes F, G and K) and explaining the data obtained by the existing and planned planet-hunting space missions[13,14,16,17]. This is a feasible task for two reasons: (1) reliable simulations of granulation patterns on main sequence stars are gradually becoming available[19,30] and (2) new methods for extrapolating the magnetically driven brightness variations from the Sun to Sun-like stars with various levels of magnetic activity observed at arbitrary angles between the rotational axis and line of sight have recently been developed[6,28].

Methods

High-cadence TSI data. We utilized TSI data obtained by the PMO6-V radiometer of the VIRGO instrument onboard the SOHO mission and by the PREMOS absolute radiometer onboard the PICARD mission (Supplementary Fig. 1) to test our model. VIRGO records TSI with 1-min cadence. Because of the failure of the shutter, the photon recording is not interrupted by the calibration procedure[31]. This was advantageous for this study, leading to a negligibly small high-frequency noise level of the VIRGO data[32]. The drawback of the shutter failure is that VIRGO is unstable on timescales from about 3–5 h to about 100 h (one can clearly see the signature of the instrumental variations on such scales in the form of excess power in Supplementary Fig. 1e–g). The amplitude of the TSI variability recorded by VIRGO at these timescales is mainly attributed to the instrumental effects (for example, it does not depend on the solar activity level). PREMOS records TSI with 2-min cadence, but unlike VIRGO it interrupts for calibration every minute. While individual PREMOS measurements are less precise than those of VIRGO, they do not suffer from the VIRGO calibration problems. Building on the complementary character of the PREMOS and VIRGO data, we created composite power spectra for three 1 month intervals using VIRGO and PREMOS on timescales below and above 3.5 h, respectively (Supplementary Fig. 1e–g).

SATIRE model. The magnetically driven TSI variability presented in this study was calculated with the SATIRE model. SATIRE decomposes the visible solar disk to magnetic features and the quiet Sun. The magnetic features are subdivided into three classes: faculae, which encompass all bright magnetic features, sunspot umbrae and sunspot penumbrae. The quiet Sun represents the part of the solar disk not covered by magnetic features. SATIRE calculates the full-disk solar brightness by weighting the fluxes from the magnetic features and the quiet Sun with their disk area coverages, taking into account the positions of the magnetic features on the solar disk.

The spectra of the magnetic features and the quiet Sun were pre-calculated[33] on a fine grid of wavelengths and disk positions using the ATLAS9 code[34,35]. The source of the information about the disk area coverages and positions of magnetic features depended on the branch of the SATIRE model. For this study, we employed SATIRE-S, which is the most accurate implementation of SATIRE. SATIRE-S infers the disk area coverages of magnetic features and their positions from full-disk solar magnetograms and continuum images[9,36].

12-min SDO/HMI magnetograms. Our modelling requires high-cadence information about the evolution of magnetic features on the visible solar disk. Such information has been available since May 2010 thanks to the SDO/HMI instrument, which simultaneously records continuum intensities and longitudinal magnetograms every 45 s. SDO/HMI data had already been used in conjunction with SATIRE-S for modelling solar variability on timescales longer than one day in a study by Yeo et al.[9]. We followed this approach, but instead of producing 315 s averages—as done by Yeo et al.[9]—we utilized the 12-min magnetograms and intensity images, which is less tedious and just as accurate.

To derive the disk area coverages of magnetic features, the 12-min SDO/HMI magnetograms were processed by the pipeline described by Yeo et al.[9], with one important exception. To avoid inconsistencies between SATIRE-S segments based on magnetograms from different instruments, Yeo et al.[9] corrected SDO/HMI magnetograms for noise using the maps of the noise level of the Michelson Doppler Imager onboard the SOHO (SOHO/MDI). These maps were calculated using an algorithm by Ortiz et al.[37]. In contrast, we directly applied the Ortiz et al.[37] algorithm to the SDO/HMI magnetograms. The noise level of SOHO/MDI is substantially higher than that of SDO/HMI, so the magnetograms reduced in this study contained more small-scale magnetic features with low magnetic flux than the magnetograms reduced by Yeo et al.[9].

The Doppler shift caused by the SDO orbital velocity[8] triggered a noticeable 24 h periodicity into the magnetic flux deduced from the HMI magnetograms and into the subsequently calculated TSI contribution by faculae (Supplementary Fig. 2a, blue lines). To account for this, we calculated the mean signature of the 24 h variations in the facular component for each of the three periods examined in this study (Supplementary Fig. 2b–d) and subtracted it from the total magnetic and facular light curves (Supplementary Fig. 2a, red lines). Since this procedure might also remove part of the real TSI variability, we plotted both power spectra (that is, those based on corrected and those based on uncorrected light curves) and compared them with the measurements (Fig. 1).

Free parameter. The SATIRE-S model has a single free parameter B_{sat}, which represents the minimum magnetogram signal from a pixel fully filled by the magnetic field[11]. If the magnetic signal in the pixel, B, is smaller than the B_{sat} value, it is assumed that the B/B_{sat} part of the pixel is covered by faculae. If B is greater than B_{sat}, the pixel is assumed to be fully covered by faculae. Yeo et al.[9] found that a B_{sat} value of 230 G optimises the agreement between the TSI output of SATIRE-S and the TSI time series obtained by the PMO6V radiometer on SOHO/VIRGO.

To determine the B_{sat} value for 12 min magnetograms, we downloaded one SDO/HMI magnetogram per day for the 30 April 2010 to 31 July 2015 period and calculated daily TSI reconstruction. A B_{sat} value of 280 G was found by optimising the agreement between our TSI reconstruction and that of Yeo et al.[9]. This value

was greater than that in Yeo et al.[9] because of the presence of a larger number of small-scale weak magnetic features in the magnetograms employed in our study.

Granulation-driven TSI variability. To quantify the variability introduced by convective motions at the solar surface, we used purely hydrodynamic simulations (that is, simulations with no magnetic field) with the MURaM[12] code. These simulations cover the upper part of the convection zone and the photosphere in cartesian boxes. To use these boxes to quantify brightness variability, we would ideally tile the solar surface in the way described by Beeck et al.[38] using a relatively long simulation covering multiple supergranules. We would then perform detailed calculations of the radiative transfer at a large number of viewing angles and combine these to obtain the strength of the fluctuations.

To test whether this full apparatus was required, we performed this detailed analysis for the small (9,000 km in both horizontal directions and 3,000 km in the vertical direction) G2V solar simulations described by Beeck et al.[19]. To save time for the purposes of the test, we used four snapshots separated in time by 19 min (making the radiative output essentially uncorrelated for these small boxes as the granulation structure had changed completely between any two snapshots). For each position, the mean and s.d. were calculated and these were used to calculate the disk-integrated average brightness and variability under the assumption that the fluctuations at different positions were uncorrelated. We found that the relative variability (defined here as the s.d. divided by the mean) was 2.05×10^{-5}. We then calculated the relative variability using the same four snapshots assuming that the variability of the flux per unit area on the disk was independent of the disk position. This yielded a variability of 1.88×10^{-5}, which is within 8% of the more detailed calculation.

On the basis of the above finding, we used the vertically emerging radiative flux from a time sequence from a large hydrodynamic simulation (196,000 km in the horizontal directions). The variability at different timescales was derived, and this was converted to a variability for the entire disk of the Sun by dividing it by a factor of $\sqrt{d^2/\pi R_\odot^2}$, where $d=196{,}000$ km.

Comparison of calculated and observed TSI variations. Using high-cadence full-disk observations from SDO/HMI, we reconstructed magnetically driven TSI variability over the three 1 month intervals considered in this study (see Table 1) with 12-min cadence. The granulation-driven TSI variability at 1-min cadence was simulated over the examined time intervals by consecutively repeating the 15 h MURaM time series. This was imposed on the magnetically driven TSI variability to yield 1-min cadence time series of magnetically and granulation-driven TSI variability.

We compared the TSI reconstruction with the 2-min cadence TSI measurements obtained by PICARD/PREMOS and the 1-min cadence TSI measurements from SOHO/VIRGO. Since variations on the 2-min timescale (which corresponded to the Nyquist frequency of 1-min cadence data) were still dominated by the p-mode oscillations and the PREMOS data were only available with 2-min cadence, we considered every second point in the synthesized and VIRGO time series.

There were gaps in the VIRGO, PREMOS and modelled time series (the latter were caused by breaks in the SDO/HMI data). In each comparison, we only considered the times at which data from all considered time series were available. For example, the wavelet power spectra in Fig. 1c,f,i were calculated utilizing only those times at which VIRGO, PREMOS and modelled data points were simultaneously present (this is the reason why the orange curves, representing the power spectrum of granulation component of TSI variability, are not identical in Fig. 1b,e,h). The proportion of the period for which all three sources of data were available was about 90% in all three considered time intervals. The gaps were filled by linearly interpolating across them.

The daily TSI values for the 'long' interval (see Table 1) were calculated following the approach of Yeo et al.[9] and compared with the observed values from the PMOD composite[27]. The latter is currently a de facto standard observational dataset and is largely based on the VIRGO data for the period considered in this study. The modelled and measured power spectra shown in Fig. 2 were obtained by merging the part covering periods of 4 min to 7 days with that covering 7 days to 19 years of the corresponding power spectra calculated for the August 2011 and 'long' intervals (see Table 1).

The ratio between the modelled and measured power spectra from Fig. 2 was plotted in Supplementary Fig. 3. We attribute deviations from unity at high frequencies to statistical noise linked to the limited duration (15 h) of the MURaM time series used in the present study. To estimate the level of this noise, we took 20 consecutive 15 h time series of PREMOS data during the first two weeks of the August 2011 interval and calculated the relative root-mean-square deviation between the power spectra of individual 15 h time series and the mean power spectrum of all the time series. As, during the 2011 interval, variability on timescales below 8 h was brought about by granulation, these deviations gave a robust 1σ estimate of the statistical errors for the ratio at the corresponding timescales. We note that deviations larger and smaller than unity had to be calculated separately to take into account that the deviations smaller than the unity were bounded at the bottom, so that the error range for the ratio was not symmetrical.

The deviations of the ratio between modelled and measured power spectra at low frequencies can be linked to the uncertainties in the available TSI data. To estimate these uncertainties, we calculated power spectra utilizing daily averaged TSI data from the PMOD[27], Active Cavity Radiometer Irradiance Monitor[39], Institut Royal Meteorologique Belgique[40] and Dudok de Wit et al.[41] TSI composites, as well as from the PREMOS/PICARD[25] and Total Irradiance Monitor instrument aboard the Solar Radiation and Climate Experiment[42] datasets. Then, we used the same algorithm as for periods below 8 h to calculate the 1σ error intervals as a function of frequency (for periods longer than 2 days). The calculations of 1σ error in the 8 h to 2 days interval were not straightforward and we refrained from performing them, assuming that the estimates on both sides of this interval gave a good estimate of the uncertainties within the interval.

We note that with a few exceptions the ratio between modelled and measured power spectra lies within the 1σ error intervals. The only significant deviation is at timescales of about 5 min and is linked to the p-mode oscillations, which are not accounted for in our model.

In Fig. 2, we also show the 1σ error of the measured power spectrum. This was calculated by attributing the 1σ error for the ratio between the modelled and measured power spectra (shown in Supplementary Fig. 3) to the error of the measured power spectrum. While the error for the ratio between modelled and measured power spectra at high frequencies was caused by the statistical noise in our simulations (and thus, strictly speaking, should be attributed to simulations), it is convenient to plot 1σ error intervals around the measured power spectrum (so that they indicate 1σ confidence intervals for the simulated power spectrum).

Our study is the first to allow replicating solar brightness variations over such a broad domain of frequencies. It is also mainly physics based, allowing us little freedom to change the properties of the granulation and magnetic variability.

Data availability. The data that support the findings of this study are available from the corresponding author on reasonable request.

Received: 9 March 2017; Accepted: 4 July 2017;
Published online: 21 August 2017

References

1. Fröhlich, C. Total solar irradiance: what have we learned from the last three cycles and the recent minimum? *Space Sci. Rev.* **176**, 237–252 (2013).
2. Kopp, G. Magnitudes and timescales of total solar irradiance variability. *J. Space Weather Spac.* **6**, A30 (2016).
3. Rabello-Soares, M. C., Roca Cortes, T., Jimenez, A., Andersen, B. N. & Appourchaux, T. An estimate of the solar background irradiance power spectrum. *Astron. Astrophys.* **318**, 970–974 (1997).
4. Ermolli, I. et al. Recent variability of the solar spectral irradiance and its impact on climate modelling. *Atmosph. Chem. Phys.* **13**, 3945–3977 (2013).
5. Solanki, S. K., Krivova, N. A. & Haigh, J. D. Solar irradiance variability and climate. *Ann. Rev. Astron. Astrophys.* **51**, 311–351 (2013).
6. Shapiro, A. I. et al. Variability of Sun-like stars: reproducing observed photometric trends. *Astron. Astrophys.* **569**, A38 (2014).
7. Meunier, N., Lagrange, A.-M., Borgniet, S. & Rieutord, M. Using the Sun to estimate Earth-like planet detection capabilities. VI. Simulation of granulation and supergranulation radial velocity and photometric time series. *Astron. Astrophys.* **583**, A118 (2015).
8. Hoeksema, J. T. et al. The Helioseismic and Magnetic Imager (HMI) vector magnetic field pipeline: overview and performance. *Sol. Phys.* **289**, 3483–3530 (2014).
9. Yeo, K. L., Krivova, N. A., Solanki, S. K. & Glassmeier, K. H. Reconstruction of total and spectral solar irradiance from 1974 to 2013 based on KPVT, SoHO/MDI, and SDO/HMI observations. *Astron. Astrophys.* **570**, A85 (2014).
10. Krivova, N. A., Solanki, S. K., Fligge, M. & Unruh, Y. C. Reconstruction of solar irradiance variations in cycle 23: is solar surface magnetism the cause? *Astron. Astrophys.* **399**, L1–L4 (2003).
11. Krivova, N. A., Solanki, S. K. & Unruh, Y. C. Towards a long-term record of solar total and spectral irradiance. *J. Atmos. Sol.-Terr. Phys.* **73**, 223–234 (2011).
12. Vögler, A. et al. Simulations of magneto-convection in the solar photosphere. Equations, methods, and results of the MURaM code. *Astron. Astrophys.* **429**, 335–351 (2005).
13. Bordé, P., Rouan, D. & Léger, A. Exoplanet detection capability of the COROT space mission. *Astron. Astrophys.* **405**, 1137–1144 (2003).
14. Borucki, W. J. et al. Kepler planet-detection mission: introduction and first results. *Science* **327**, 977–980 (2010).
15. Basri, G., Walkowicz, L. M. & Reiners, A. Comparison of Kepler photometric variability with the Sun on different timescales. *Astrophys. J.* **769**, 37 (2013).
16. Ricker, G. R. et al. Transiting Exoplanet Survey Satellite (TESS). *J. Astron. Telesc. Instrum. Syst.* **1**, 014003 (2015).
17. Rauer, H. et al. The PLATO 2.0 mission. *Exper. Astron.* **38**, 249–330 (2014).

18. Schou, J. et al. Design and ground calibration of the Helioseismic and Magnetic Imager (HMI) instrument on the Solar Dynamics Observatory (SDO). *Sol. Phys.* **275**, 229–259 (2012).
19. Beeck, B., Cameron, R. H., Reiners, A. & Schüssler, M. Three-dimensional simulations of near-surface convection in main-sequence stars. II. Properties of granulation and spectral lines. *Astron. Astrophys.* **558**, A49 (2013).
20. Aigrain, S., Favata, F. & Gilmore, G. Characterising stellar micro-variability for planetary transit searches. *Astron. Astrophys.* **414**, 1139–1152 (2004).
21. Seleznyov, A. D., Solanki, S. K. & Krivova, N. A. Modelling solar irradiance variability on time scales from minutes to months. *Astron. Astrophys.* **532**, A108 (2011).
22. Rast, M. P. The scales of granulation, mesogranulation, and supergranulation. *Astrophys. J.* **597**, 1200–1210 (2003).
23. Solanki, S. K., Inhester, B. & Schüssler, M. The solar magnetic field. *Rep. Progr. Phys.* **69**, 563–668 (2006).
24. Bastien, F. A., Stassun, K. G., Basri, G. & Pepper, J. An observational correlation between stellar brightness variations and surface gravity. *Nature* **500**, 427–430 (2013).
25. Schmutz, W., Fehlmann, A., Finsterle, W., Kopp, G. & Thuillier, G. Total solar irradiance measurements with PREMOS/PICARD. *AIP Conf. Proc.* **1531**, 624–627 (2013).
26. Fröhlich, C. et al. VIRGO: experiment for helioseismology and solar irradiance monitoring. *Sol. Phys.* **162**, 101–128 (1995).
27. Fröhlich, C. Solar irradiance variability since 1978. Revision of the PMOD composite during solar cycle 21. *Space Sci. Rev.* **125**, 53–65 (2006).
28. Shapiro, A. I., Solanki, S. K., Krivova, N. A., Yeo, K. L. & Schmutz, W. K. Are solar brightness variations faculae- or spot-dominated? *Astron. Astrophys.* **589**, A46 (2016).
29. Aigrain, S. et al. Testing the recovery of stellar rotation signals from Kepler light curves using a blind hare-and-hounds exercise. *Mon. Not. R. Astron. Soc.* **450**, 3211–3226 (2015).
30. Ludwig, H.-G. et al. Hydrodynamical simulations of convection-related stellar micro-variability. II. The enigmatic granulation background of the CoRoT target HD 49933. *Astron. Astrophys.* **506**, 167–173 (2009).
31. Fröhlich, C. et al. First results from VIRGO, the experiment for helioseismology and solar irradiance monitoring on SOHO. *Sol. Phys.* **170**, 1–25 (1997).
32. Fröhlich, C. & Lean, J. Solar radiative output and its variability: evidence and mechanisms. *Astron. Astrophys. Rev.* **12**, 273–320 (2004).
33. Unruh, Y. C., Solanki, S. K. & Fligge, M. The spectral dependence of facular contrast and solar irradiance variations. *Astron. Astrophys.* **345**, 635–642 (1999).
34. Kurucz, R. L. "Finding" the "missing" solar ultraviolet opacity. *Rev. Mex. Astron. Astrof.* **23**, 181–186 (1992).
35. Castelli, F. & Kurucz, R. L. Model atmospheres for VEGA. *Astron. Astrophys.* **281**, 817–832 (1994).
36. Ball, W. T., Krivova, N. A., Unruh, Y. C., Haigh, J. D. & Solanki, S. K. A new SATIRE-S spectral solar irradiance reconstruction for solar cycles 21–23 and its implications for stratospheric ozone. *J. Atmos. Sci.* **71**, 4086–4101 (2014).
37. Ortiz, A., Solanki, S. K., Domingo, V., Fligge, M. & Sanahuja, B. On the intensity contrast of solar photospheric faculae and network elements. *Astron. Astrophys.* **388**, 1036–1047 (2002).
38. Beeck, B., Cameron, R. H., Reiners, A. & Schüssler, M. Three-dimensional simulations of near-surface convection in main-sequence stars. I. Overall structure. *Astron. Astrophys.* **558**, A48 (2013).
39. Willson, R. C. & Mordvinov, A. V. Secular total solar irradiance trend during solar cycles 21–23. *Geophys. Res. Lett.* **30**, 3–1 (2003).
40. Dewitte, S., Crommelynck, D., Mekaoui, S. & Joukoff, A. Measurement and uncertainty of the long-term total solar irradiance trend. *Sol. Phys.* **224**, 209–216 (2004).
41. Dudok de Wit, T., Kopp, G., Fröhlich, C. & Schöll, M. Methodology to create a new total solar irradiance record: making a composite out of multiple data records. *Geophys. Res. Lett.* **44**, 1196–1203 (2017).
42. Kopp, G., Lawrence, G. & Rottman, G. The Total Irradiance Monitor (TIM): science results. *Sol. Phys.* **230**, 129–139 (2005).

Acknowledgements

The authors received funding from the People Programme (Marie Curie Actions) of the European Union's Seventh Framework Programme (FP7/2007-2013) under grant agreement No. 624817 and the European Research Council under the European Union's Horizon 2020 research and innovation programme (grant agreement No. 715947). Financial support was also provided by the Brain Korea 21 plus program through the National Research Foundation funded by the Ministry of Education of Korea and by the German Federal Ministry of Education and Research under project 01LG1209A. We would like to thank the International Space Science Institute, Bern, for their support of science team 373 and the resulting helpful discussions.

Author contributions

A.I.S., S.K.S. and N.A.K. designed the study. A.I.S. performed the calculations with contributions from R.H.C., who provided the MURaM time series, and K.L.Y., who prepared the HMI/SDO magnetograms and corrected them for noise. N.A.K. and S.K.S. led the development of the SATIRE code. R.H.C. actively contributed to the development of the MURaM code. W.K.S. provided the PREMOS data and expertise on the TSI data. A.I.S., S.K.S., N.A.K. and R.H.C. wrote the paper.

Competing interests

The authors declare no competing financial interests.

Additional information

Supplementary information is available for this paper at doi:10.1038/s41550-017-0217-y.

Reprints and permissions information is available at www.nature.com/reprints.

Correspondence and requests for materials should be addressed to A.I.S.

Publisher's note: Springer Nature remains neutral with regard to jurisdictional claims in published maps and institutional affiliations.